This is the accepted manuscript made available via CHORUS. The article has been published as:

Spin-orbit coupling and interactions in quantum Hall states of graphene/math xmlns="http://www.w3.org/1998/Math/MathML">msub>mi>WSe/mi>mn>2/mn>/msub>/math> heterobilayers

Dongying Wang, Mohammed Karaki, Nicholas Mazzucca, Haidong Tian, Guixin Cao, ChunNing Lau, Yuan-Ming Lu, Marc Bockrath, Kenji Watanabe, and Takashi Taniguchi

Phys. Rev. B **104**, L201301 — Published 19 November 2021

DOI: 10.1103/PhysRevB.104.L201301

Spin-orbit coupling and interactions in quantum Hall states of graphene/WSe_2 heterobilayers

Dongying Wang, Mohammed Karaki, Nicholas Mazzucca, Haidong Tian, Guixin Cao, ChunNing Lau, Yuan-Ming Lu, and Marc Bockrath*
Department of Physics, The Ohio State University, Columbus, OH 43210, USA

Kenji Watanabe
Research Center for Functional Materials, National Institute for Materials Science, 1-1 Namiki, Tsukuba 305-0044, Japan

Takashi Taniguchi
International Center for Materials Nanoarchitectonics, National Institute for Materials Science, 1-1 Namiki, Tsukuba 305-0044, Japan

(Dated: October 28, 2021)

We use magnetotransport measurements to probe quantum Hall ground states in graphene/WSe_2 heterobilayers. Compared to pristine graphene, inter-Landau level (LL) gaps at half-filled quartets away from filling factor $\nu = 0$ show significantly weaker dependence on the magnetic field B, while odd ν fillings show a stronger dependence. We interpret this behavior using a model incorporating Ising and Rashba spin-orbit coupling (SOC) along with Coulomb interactions within the self-consistent Hartree-Fock framework. A model fit yields Ising SOC in range $1 \sim 2$ meV, Rashba $\sim$10 meV, and the in-plane dielectric constant $\sim$12, in agreement to previously found values. In the zeroth LL quartet, the $\nu = 0$ gap as a function of magnetic field exhibits a plateau near 5 T, compared to $\sim 20 - 25$ T for pristine graphene. This behavior is in agreement with a model in which the SOC causes a phase transition from a canted antiferromagnetic state to a ferromagnetic state to occur at a much lower field. Our studies demonstrate how the interplay of SOC and electronic interactions affect graphene's electronic structure.

Spin-orbit coupling (SOC) provides a promising route to controlling spin degrees of freedom in devices as well as realizing topological phases [1, 2]. Graphene has emerged as a high mobility material with outstanding electronic properties. However its intrinsic SOC is weak [3–6]. This has motivated many proposals and studies to induce SOC in graphene using proximity to other materials with stronger SOCs[7–24]. These include adatoms [7, 8] as well as other 2D materials such as transition metal dichalcogenides [9–18] (TMDs). Previous works have shown that coupling graphene to TMDs induces a SOC that can be detected from weak localization [11–16] and Shubnikov de Haas oscillations [13]. Moreover, coupling graphene to TMDs has the advantage of retaining graphenes high mobility. Recent work has shown that SOC can be measured from the quantum Hall effect (QHE) [17, 18], where both valley Zeeman and Rashba SOC can be measured in the same device [17].

Because of electronic interactions, the QHE in mono- and few-layer graphene exhibits a rich phase diagram with various spin, valley, and layer orderings [25, 26]. These symmetry-breaking interactions lift the degeneracy between quartets of Landau levels (LLs) in graphene [27, 28]. As SOC splits the spin degeneracy and breaks inversion symmetry, it is expected to profoundly influence the many-body phases in graphene. However, a comprehensive study on graphene quantum Hall effects, where both the SOC and interactions play important roles, has not been performed.

Here we report quantum Hall studies of monolayer graphene/monolayer tungsten diselenide (WSe_2) structures encapsulated in hexagonal boron nitride (hBN). At low temperatures, within a perpendicular magnetic field B, we observe a Landau fan showing all integer quantum Hall states, which provides information of the spin and valley symmetry-breaking gaps. To investigate the LL structure with the influence of proximity-induced SOC, we use temperature-dependent transport measurements to determine the inter-LL gaps Δ_ν associated with the broken symmetry states in the QHE. All gaps increase with B with different characteristic slopes for electron and hole doping, deviating from the isolated graphene behavior [29]. A single-particle continuum model based on Dirac fermions with an out-of-plane Ising and in-plane Rashba SOCs is unable to account for the observed trends. We therefore include electron-electron interactions in a self-consistent Hartree-Fock approach. A good fit of the B-dependent gap behavior to the Hartree-Fock model is obtained, enabling us to extract the SOC parameters and the effective dielectric constant. In the zeroth LL, due to minimal screening of the Coulomb interaction at charge neutrality, the Hartree-Fock approach cannot capture the strong electronic interaction and fails to provide a satisfactory fit to the experimental data.

The longitudinal resistance as well as the measured gap vs. magnetic field both show a plateau near $B =$ 5 T. This is consistent with a field-induced transition from a canted antiferromagnetic state to a ferromagnetic

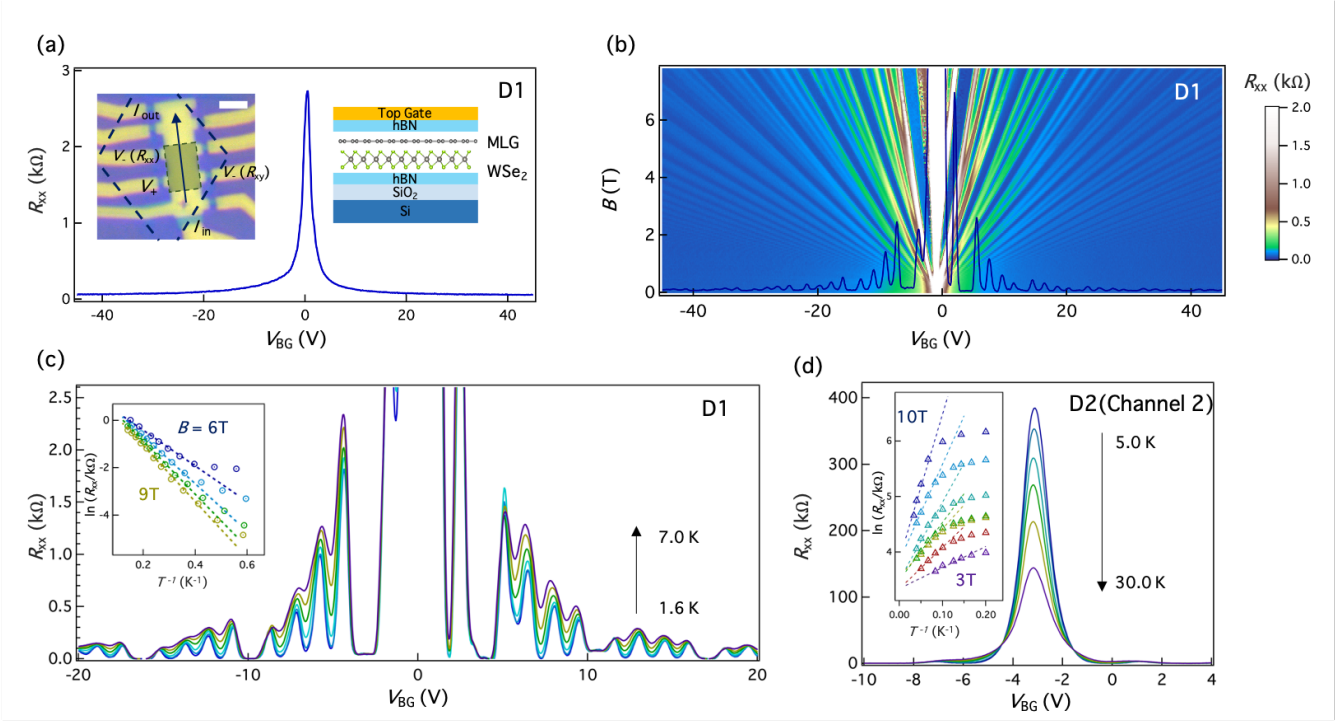


FIG. 1. **All-integer quantum Hall effect in monolayer graphene on WSe_2.** (a) Main panel: R_{xx} versus V_{BG} at $T = 1.5$ K. Left inset: Optical image of an MLG/WSe_2 device. The dark blue dashed outline indicates the WSe_2 region before etching. Labels are included to indicate the current and voltage probes in use and the applied current direction is shown with the arrow. Green highlighted region is the measured area. Scale bar is 1.5 μm. Right inset: Schematic diagram of the layer stack. (b) Landau Fan from a monolayer graphene on WSe_2 device. Splitting of the quartet LLs is visible above 3 T and quantum Hall gaps at all integer fillings become visible at 8 T (superimposed). (c) Temperature dependence of R_{xx} minima in symmetry broken quantum Hall states at $B = 9$ T. Inset: Arrhenius plot for $\nu = 4$ as a function of magnetic field. (d) Temperature dependence of the insulating state at $\nu = 0$ at $B = 9$ T. Inset: Arrhenius plot for $\nu = 0$ as a function of magnetic field.

state [29, 30], in which SOC drives this transition to a much lower magnetic field compared to that found in previous studies on isolated graphene [31–33]. A similar observation has been reported in monolayer graphene in proximity to yttrium iron garnet (YIG) [34]. However, here we demonstrate that such behavior can occur in the absence of magnetic materials.

Our devices were fabricated using a dry transfer and stacking method [35]. Graphene and WSe_2 flakes were first exfoliated on SiO_2/Si substrates (285 nm thick SiO_2) and then brought together and encapsulated in two hBN layers. After vacuum annealing and contact mode AFM cleaning [36], conventional electron beam lithography, and reactive ion etching techniques were employed to pattern multi-terminal Hall bar geometry. A 5 nm/70 nm Cr/Au metal layer were then evaporated to make one-dimensional edge contacts [37]. The degenerately doped Si substrate acts as a back gate. The Fig. 1a left inset shows an optical image of a completed device as well as the measurement configuration. The right inset shows the layer stacking diagram. (We also employed a metal top gate to study the effects of displacement field, which shows no obvious influence, see Fig. 2b in Supplemental Information [38].)

We obtained high-quality data from two separate monolayer graphene/monolayer WSe_2 devices, D1 and D2. To perform the measurements, completed devices were loaded into a variable-temperature flowing gas ^{4}He cryostat. Transport measurements were performed at a base temperature $T = 1.6$ K using low-frequency lock-in techniques with a constant ac current of 50 nA. Within the whole measurement range, the Fermi level of WSe_2 is in its bandgap [39]. All conducting signals we observed came from the graphene layer. In the Fig. 1a main panel, we show the longitudinal resistance R_{xx} as function of back gate voltage V_{BG} (applied to the Si layer) from a representative device. From the Drude model, we extract the field mobility to be 120,000 $cm^2V^{-1}s^{-1}$ at low temperature, indicating the high quality of our sample. With a perpendicular magnetic field B applied, a color plot of R_{xx} versus V_{BG} and B shows a Landau fan pattern (Fig. 1b), arising from the integer QHE of graphene. Consistent with the QHE in pristine monolayer graphene, the primary gaps occur at filling factors $\nu = 4(n+1/2)$, where n is the Landau level orbital index [40]. At those filling factors, the longitudinal resistance valleys show flat behavior near zero, while the transverse resistance shows well-developed

plateaus at the appropriate quantized values as shown in Supplemental (Fig. 2a) [38]. 4-fold degenerate LLs due to the spin and valley degeneracy can be split by perturbations such as electronic interactions and Zeeman splitting, as well as the proximity-induced SOC in our devices. Symmetry breaking gaps at half fillings of the nearly-degenerate quartets (such as $\nu = \pm 4, 8, 12, \dots$) begin to appear above $B = 3$ T. For $B > 6$ T, R_{xx} minima are visible at all integer QHE states. A line trace for R_{xx} as a function of $V_{\rm BG}$ at $B = 8$ T is overlaid.

To determine the effect of the SOC on the LL spectrum, we determined the thermal activation gaps Δ_ν by measuring the temperature dependence of R_{xx} minima at a number of filling factors. These gaps are associated with the energy cost of the lowest-lying charged excitations of the ground state. The Δ_ν measurements enable us to extract quantitative information of the symmetry broken gaps in the presence of proximity-induced SOC. Examples of these measurements are shown in Figs. 1c and 1d. The insets show Arrhenius plots for $\nu = 4$ (1c inset) and $\nu = 0$ (1d inset).

We begin our discussion with the evolution of symmetry broken gaps with the magnetic field. At very low perpendicular fields, R_{xx} minima are visible only at half quartet fillings, $\nu = \pm 4, 8, 12, \dots$. Minima at quarter fillings of each quartet emerge and become deeper with increasing B. Fig. 2a shows a log plot of R_{xx} versus $V_{\rm BG}$ at $B = 8$ T. For electron doping, R_{xx} minima at half quartet fillings are much deeper than minima at quarter fillings. The opposite holds true for hole doping for $n \geq 2$. Measured activation gaps vs. B for the 1st LL quartet are shown as open circles in Fig. 2b and 2c. The B-dependence of Δ_ν for all filling factors is similar, following an approximately linear scaling, except for $\nu = -4$. The hole side half-filled quartet LL gap, Δ_{-4}, grows more slowly with B, saturating eventually above 9 T. This trend becomes more pronounced for higher LL index ($\nu = -8, -12$, see Fig. S3 in SI). In contrast, the half-filled quartet gaps in isolated graphene scale linearly with B with an enhanced g-factor, resulting from exchange contributions[29]. Here we attribute the saturating behavior of these gaps observed in our samples to proximity induced SOCs.

To understand the impact of SOC on the LL structure and extracting the SOC parameters from the gaps, we start from a single-particle continuum Dirac model incorporating Rashba and Ising SOCs, parametrized by λ and V respectively. Below is the non-interacting Dirac Hamiltonian considered in this work:

$$H = v_F(\tau_z\sigma_x\hat{\pi}_x + \sigma_y\hat{\pi}_y) + \frac{\lambda}{2}(\tau_z s_y\sigma_x - s_x\sigma_y) + V\tau_z s_z + b s_z, \quad (1)$$

where $v_F = 1 \times 10^6$ m/s is the Fermi velocity, and τ_i, s_i, σ_i denote the Pauli matrices for the valley, spin and sublattice degrees of freedom, and $\hat{\boldsymbol{\pi}} = -i\hbar\nabla + e\boldsymbol{A}$ is the momentum operator, where $b = g\mu B/2$ is the Zeeman

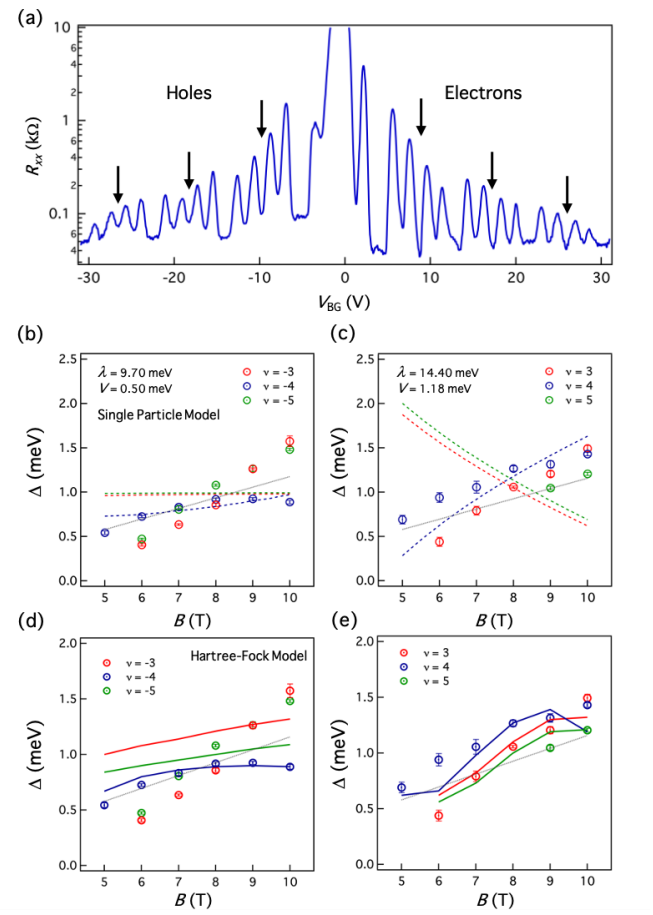


FIG. 2. **Symmetry-broken quantum Hall states and theoretical fitting results.** (a) R_{xx} vs. $V_{\rm BG}$ taken at $B = 8$ T in a log scale. (b, c) Measured thermal activation gaps (open circles) and single particle fitting results (dashed lines) for $\nu = -3, -4, -5$ and $\nu = 3, 4, 5$. (d, e) Measured thermal activation gaps (open circles) for $\nu = \pm 3, \pm 4, \pm 5$ as well as the corresponding Hartree-Fock fitting results (solid lines). Gray dotted lines represent the Zeeman splitting with $g = 2$. Within each LL quartet, the fitting parameters for the even and odd filling factors are obtained separately. Data in this figure are all collected from sample D1.

splitting. This single-particle model preserves two $U(1)$ symmetries generated by valley (τ_z) and sublattice-spin ($s_z\sigma_z$) rotations. The anti-unitary particle-hole symmetry, generated by $\mathcal{C} = \sigma_z \cdot \mathcal{K}$ where $\mathcal{K}$ stands for complex conjugation, is explicitly broken by the Ising SOC ($\propto V$) and Zeeman term ($\propto b$). This symmetry breaking carries over when interactions are incorporated in the model, and it is manifested in the particle-hole asymmetry of activation gaps.

We have performed a fit for the measured gaps in each LL quartet. The results showed that this single-particle Hamiltonian does not capture more than one gap in each LL, as shown in Fig. 2b and 2c. We therefore incorporate the effects of Coulomb interactions via a Hartree-Fock

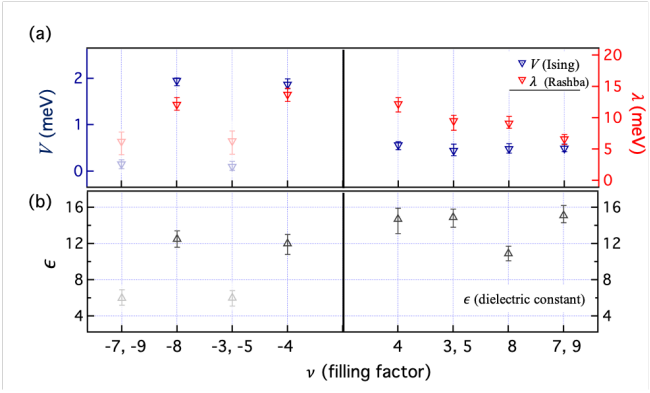


FIG. 3. **Extracted SOC strength with Coulomb interactions incorporated in a self-consistent Hartree-Fock calculation.** The Rashba and Ising SOC parameters (a) and the dielectric constant (b) from the Hartree-Fock fitting of the thermal activation gaps in each LL are considered separately. Hartree-Fock fitting results for negative odd filling shown in lighter colors are less accurate, likely due to less screened Coulomb interactions at odd fillings compared to even ones.

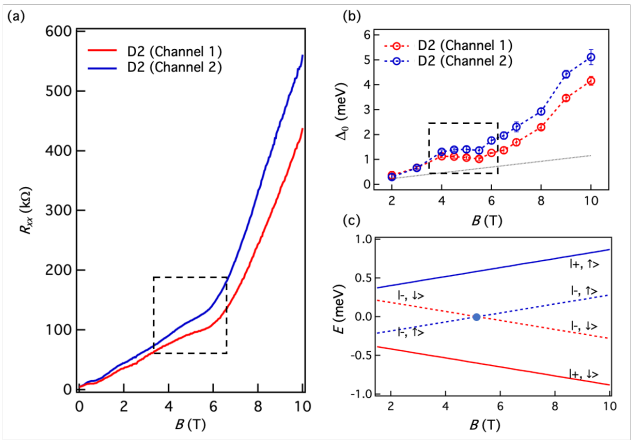


FIG. 4. **Quantum Hall states near the charge neutral point.** (a) Longitudinal resistance R_{xx} as a function of magnetic field B. (b) Measured thermal activation gap for $\nu = 0$. Gray dotted lines represent the Zeeman splitting with $g = 2$. (c) Simulated zero energy LL structure in single particle model with $V = 0.3$ meV. Valley and spin information is noted for each LL branch. Data in this figure are collected from D2.

approximation [41], characterized by an in-plane dielectric constant ϵ.

Fig. 2d and 2e show the calculated gaps plotted against B (solid lines) along with the data (open circles) for $\nu = -3$, -4, and -5 in the left panel and $\nu = 3$, 4, and 5 in the right panel. Both the characteristic value of the slope $d\Delta_\nu/dB$ for positive odd ν, as well as the saturating behavior at half quartet filling, are captured by the fits. On the hole side, the Hartree-Fock fits (e.g. the slope of $\Delta(B)$ curve) for odd ν do not match the data as well as the even ν fits. Since the small $|\vec{q}|$ intravalley Coulomb interaction between electrons of opposite spins dominates over the intervalley one, it screens better in the high-field ferromagnetic ground state at the even fillings than the odd fillings. Therefore it is less likely for the Hartree-Fock approximation to produce accurate results at an odd filling factor. The Rashba term, which contributes to the energy a term proportional to $1/\sqrt{B}$, can result in a saturation behaviour of the gaps at large fields, as is observed at even, negative filling factors in the experimental data.

Fig. 3 shows the obtained fit parameters for a number of different filling factors. These values appear consistent for the different quartets. We find an Ising SOC in range $\sim 1-2$ meV, a Rashba SOC $\sim$12 meV, and a dielectric constant $\sim$12, consistent with previous measurements [11–18]. It is worth mentioning that the SOC fitting parameters extracted from the data shows an electron-hole asymmetry, indicating the possible gate tunability of SOC strength. This is consistent with observed larger Ising SOC in valence bands of TMD compared to conduction bands [42–45]. Moreover, while monolayer hBNs dielectric constant is $\epsilon_{\parallel,1} \approx 6.8$, the dielectric constant of monolayer WSe_2 is $\epsilon_{\parallel,2} \approx 15.3$ [46], yielding a characteristic environmental dielectric constant $\bar{\epsilon}_\parallel = (\epsilon_{\parallel,1} + \epsilon_{\parallel,2})/2 \approx 11$ in reasonable agreement to the obtained value.

We now turn to the behavior of the zeroth LL quartet. A further notable feature of the experimental data is the plateau behavior of R_{xx} and Δ_0 near $B = 5$ T. Fig. 4a shows the longitudinal resistance R_{xx} as a function of B at charge neutrality. R_{xx} generally increases with B. An obvious slope decrease takes place around $B = 5$ T, as shown in the dashed box. To further look into the $\nu = 0$ quantum Hall state, we extract its thermal activation gap Δ_0, according to the equation, $R_{xx} = R_0 e^{\Delta_0/2k_BT}$ (shown in Fig. 4b). Consistent with the evolution of the longitudinal resistance, at $B = 5$ T, the gap size stops increasing and stabilizes around 1.2 meV, and then increases again as the field continuously increasing. This observation deviates from previous results in isolated graphene, where an interaction-induced $\nu = 0$ gap shows a square root or sub-linear dependence with magnetic field [29, 47, 48]. We attribute this behavior to a LL crossing induced by B, which is already visible in the single particle model without Hartree-Fock corrections. As illustrated by Fig. 4c, as the magnetic field increases, the Zeeman terms drives the spin up LLs to decrease and the spin down LLs to increase in energy, resulting in a LL crossing of states with opposite spin in the K_- valley at $B \approx 5$ T. This indicates a phase transition from a canted anti-ferromagnetic state into a ferromagnetic state, leading to a kink in the transport gap Δ_0 as a function of magnetic field B as observed in Fig. 4b. The critical B at which this transition occurs depends on the SOC strength in the single particle model and can be modified by the Coulomb interaction.

In summary, we measured inter-Landau level activation gaps in WSe_2/graphene heterostructures via transport

measurements versus perpendicular magnetic field, and fit their behavior to a Dirac model including spin-orbit coupling in Coulomb interactions. We obtained values for the Ising and Rashba SOCs consistent with previous measurements. The behavior of the longitudinal resistivity in the zeroth Landau level shows a marked departure from the behavior found in pristine graphene. This can be understood as a transition from an canted anti-ferromagnetic to ferromagnetic a state that occurs at a low magnetic field because of the SOC. Future work, including parallel magnetic field measurements, is likely to yield additional insight into the interplay of SOC and interactions in 2D materials.

The experimental work is supported by NSF under award number DMR-2004801 (DW, MB).The theoretical work is supported by NSF under award number DMR-1653769 (MK,YML). Growth of hexagonal boron nitried crystals was supported by the Elemental Strategy Initiative conducted by the MEXT, Japan (Grant Number JPMXP0112101001) and JSPS KAKENHI (Grant Numbers 19H05790 and JP20H00354).

* bockrath.31@osu.edu

[1] M. Z. Hasanand C. L. Kane, Rev. Mod. Phys. **82**, 3045 (2010).
[2] A. Manchon, H. C. Koo, J. Nitta, S. M. Frolov, and R. A. Duine, Nat. Mater. **14**, 871 (2015).
[3] J. C. Boettgerand S. B. Trickey, Phys. Rev. B **75**, 121402 (2007).
[4] S. Konschuh, M. Gmitra, D. Kochan, and J. Fabian, Phys. Rev. B **85**, 115423 (2012).
[5] R. van Gelderenand C. M. Smith, Phys. Rev. B **81**, 125435 (2010).
[6] J. Sichau, M. Prada, T. Anlauf, T. J. Lyon, B. Bosnjak, L. Tiemann, and R. H. Blick, Phys. Rev. Lett. **122**, 046403 (2019).
[7] J. Balakrishnan, G. Kok Wai Koon, M. Jaiswal, A. H. Castro Neto, and B. Özyilmaz, Nat. Phys. **9**, 284 (2013).
[8] D. Marchenko, A. Varykhalov, M. R. Scholz, G. Bihlmayer, E. I. Rashba, A. Rybkin, A. M. Shikin, and O. Rader, Nat. Commun. **3**, 1232 (2012).
[9] A. Avsar, J. Y. Tan, T. Taychatanapat, J. Balakrishnan, G. K. W. Koon, Y. Yeo, J. Lahiri, A. Carvalho, A. S. Rodin, E. C. T. O'Farrell, G. Eda, A. H. Castro Neto, and B. Özyilmaz, Nat. Commun. **5**, 4875 (2014).
[10] L. A. Benítez, J. F. Sierra, W. Savero Torres, A. Arrighi, F. Bonell, M. V. Costache, and S. O. Valenzuela, Nat. Phys. **14**, 303 (2018).
[11] Z. Wang, D.-K. Ki, J. Y. Khoo, D. Mauro, H. Berger, L. S. Levitov, and A. F. Morpurgo, Phys. Rev. X **6**, 041020 (2016).
[12] Z. Wang, D. Ki, H. Chen, H. Berger, A. H. MacDonald, and A. F. Morpurgo, Nat. Commun. **6**, 8339 (2015).
[13] B. Yang, M.-F. Tu, J. Kim, Y. Wu, H. Wang, J. Alicea, R. Wu, M. Bockrath, and J. Shi, 2D Mater. **3**, 031012 (2016).
[14] B. Yang, M. Lohmann, D. Barroso, I. Liao, Z. Lin, Y. Liu, L. Bartels, K. Watanabe, T. Taniguchi, and J. Shi, Phys. Rev. B **96**, 041409 (2017).
[15] T. Wakamura, F. Reale, P. Palczynski, S. Guéron, C. Mattevi, and H. Bouchiat, Phys. Rev. Lett. **120**, 106802 (2018).
[16] S. Zihlmann, A. W. Cummings, J. H. Garcia, M. Kedves, K. Watanabe, T. Taniguchi, C. Schönenberger, and P. Makk, Phys. Rev. B **97**, 075434 (2018).
[17] D. Wang, S. Che, G. Cao, R. Lyu, K. Watanabe, T. Taniguchi, C. N. Lau, and M. Bockrath, Nano Lett. **19**, 7028 (2019).
[18] J. O. Island, X. Cui, C. Lewandowski, J. Y. Khoo, E. M. Spanton, H. Zhou, D. Rhodes, J. C. Hone, T. Taniguchi, K. Watanabe, L. S. Levitov, M. P. Zaletel, and A. F. Young, Nature 10.1038/s41586-019-1304-2 (2019).
[19] M. M. Asmarand S. E. Ulloa, Phys. Rev. B **91**, 165407 (2015).
[20] M. Gmitraand J. Fabian, Phys. Rev. B **92**, 155403 (2015).
[21] M. Gmitraand J. Fabian, Phys. Rev. Lett. **119**, 146401 (2017).
[22] J. Y. Khooand L. Levitov, Phys. Rev. B **98**, 115307 (2018).
[23] J. Y. Khoo, A. F. Morpurgo, and L. Levitov, Nano Lett. **17**, 7003 (2017).
[24] A. De Martino, A. Hütten, and R. Egger, Phys. Rev. B **84**, 155420 (2011).
[25] M. O. Goerbig, R. Moessner, and B. Douçot, Phys. Rev. B **74**, 161407 (2006).
[26] J. Aliceaand M. P. Fisher, Solid State Commun. **143**, 504 (2007).
[27] K. Nomuraand A. H. MacDonald, Phys. Rev. Lett. **96**, 256602 (2006).
[28] Y. Zhang, Z. Jiang, J. P. Small, M. S. Purewal, Y.-W. Tan, M. Fazlollahi, J. D. Chudow, J. A. Jaszczak, H. L. Stormer, and P. Kim, Phys. Rev. Lett. **96**, 136806 (2006).
[29] A. F. Young, C. R. Dean, L. Wang, H. Ren, P. Cadden-Zimansky, K. Watanabe, T. Taniguchi, J. Hone, K. L. Shepard, and P. Kim, Nat. Phys. **8**, 550 (2012).
[30] M. Kharitonov, Phys. Rev. B **85**, 155439 (2012).
[31] P. Maher, C. R. Dean, A. F. Young, T. Taniguchi, K. Watanabe, K. L. Shepard, J. Hone, and P. Kim, Nature Physics **9**, 154 (2013).
[32] A. Young, J. Sanchez-Yamagishi, B. Hunt, S. Choi, K. Watanabe, T. Taniguchi, R. Ashoori, and P. Jarillo-Herrero, Nature **505**, 528 (2014).
[33] F. Chiappini, S. Wiedmann, K. Novoselov, A. Mishchenko, A. K. Geim, J. C. Maan, and U. Zeitler, Phys. Rev. B **92**, 201412 (2015).
[34] Y. Li, M. Amado, T. Hyart, G. P. Mazur, V. Risinggård, T. Wagner, L. McKenzie-Sell, G. Kimbell, J. Wunderlich, J. Linder, and J. W. A. Robinson, Phys. Rev. B **101**, 241405 (2020).
[35] C. R. Dean, A. F. Young, I. Meric, C. Lee, L. Wang, S. Sorgenfrei, K. Watanabe, T. Taniguchi, P. Kim, K. L. Shepard, and J. Hone, Nat. Nano. **5**, 722 (2010).
[36] M. R. Rosenberger, H.-J. Chuang, K. M. McCreary, A. T. Hanbicki, S. V. Sivaram, and B. T. Jonker, ACS Appl. Mater. Interfaces **10**, 10379 (2018).
[37] L. Wang, I. Meric, P. Y. Huang, Q. Gao, Y. Gao, H. Tran, T. Taniguchi, K. Watanabe, L. M. Campos, D. A. Muller, J. Guo, P. Kim, J. Hone, K. L. Shepard, and C. R. Dean, Science **342**, 614 (2013).
[38] See Supplemental Material at [URL will be inserted by publisher] for additional experimental and theoretical

results.
[39] K. Kim, S. Larentis, B. Fallahazad, K. Lee, J. Xue, D. C. Dillen, C. M. Corbet, and E. Tutuc, ACS Nano **9**, 4527 (2015).
[40] Y. Zhang, Y.-W. Tan, H. L. Stormer, and P. Kim, Nature **438**, 201 (2005).
[41] X.-Z. Yanand C. S. Ting, Phys. Rev. B **95**, 075107 (2017).
[42] G.-B. Liu, W.-Y. Shan, Y. Yao, W. Yao, and D. Xiao, Phys. Rev. B **88**, 085433 (2013).
[43] K. Kośmider, J. W. González, and J. Fernández-Rossier, Phys. Rev. B **88**, 245436 (2013).
[44] H. Yuan, M. S. Bahramy, K. Morimoto, S. Wu, K. Nomura, B.-J. Yang, H. Shimotani, R. Suzuki, M. Toh, C. Kloc, *et al.*, Nature Physics **9**, 563 (2013).
[45] H. Zeng, G.-B. Liu, J. Dai, Y. Yan, B. Zhu, R. He, L. Xie, S. Xu, X. Chen, W. Yao, *et al.*, Scientific reports **3**, 1 (2013).
[46] A. Laturia, M. L. Van de Put, and W. G. Vandenberghe, npj 2D Materials and Applications **2**, 6 (2018).
[47] D. A. Abanin, B. E. Feldman, A. Yacoby, and B. I. Halperin, Phys. Rev. B **88**, 115407 (2013).
[48] B. Roy, M. P. Kennett, and S. Das Sarma, Phys. Rev. B **90**, 201409 (2014).